




# Microstructure and Mechanical Properties of Al/MgAl<sub>2</sub>O<sub>4</sub> In Situ Composites Synthesized by Ultrasonic Cavitation

R. Raghu<sup>1</sup> · Jayakrishnan Nampoothiri<sup>2,3</sup> · T. Satish Kumar<sup>3</sup>  · R. Subramanian<sup>3</sup>

Received: 17 September 2018 / Accepted: 3 January 2019 / Published online: 29 January 2019  
© The Indian Institute of Metals - IIM 2019

**Abstract** Al–4Mg/MgAl<sub>2</sub>O<sub>4</sub> composites were successfully synthesized by the in situ reaction of Al–4Mg alloy melt and H<sub>3</sub>BO<sub>3</sub> precursor in the presence of ultrasonic cavitation field. Ultrasonic-assisted synthesis facilitated generation of ~ 350-nm-sized MgAl<sub>2</sub>O<sub>4</sub> particles. Enhanced reaction along with dispersion of MgAl<sub>2</sub>O<sub>4</sub> was perceived due to the synergetic effect of ultrasonic cavitation. The presence of MgAl<sub>2</sub>O<sub>4</sub> particles resulted in 3–4 times reduction in matrix alloy grain size, and the grain refinement was further enhanced by ultrasonic treatment. Compared to unreinforced alloy, ultrasonicated Al/MgAl<sub>2</sub>O<sub>4</sub> composite exhibited an improvement in ultimate tensile strength by ~ 30 MPa with ~ 85% of ductility retention. Grain boundary strengthening, Orowan dispersion strengthening, coefficient of thermal expansion mismatch strengthening and load-bearing strengthening were the anticipated mechanism for enhancement in mechanical properties.

**Keywords** Al–Mg alloy · MgAl<sub>2</sub>O<sub>4</sub> · Grain refinement · Ultrasonic treatment · Mechanical properties

## 1 Introduction

Aluminium alloys are gaining greater importance in automotive and aerospace industries since they possess low density, better specific strength and high specific stiffness. However, owing to their deficient mechanical properties, the range of application is limited. Grain refinement technique is used for improving the mechanical properties of aluminium alloys. Grain refinement technique is employed to produce uniform, equiaxed and fine grains in the aluminium alloys for numerous years [1–3]. Smaller grains provide structural uniformity and consequently better strength along with reduction in porosity, hot tearing and macro-segregation [4, 5]. Even though several grain refinement methods are widely used to refine aluminium alloys, addition of inoculants as grain refiners is used extensively to refine the grains [6]. Amongst various grain refiners, Al–Ti–B master alloys are the easily accessible potential refiners at industrial scale [7]. But release of fluoride and chloride gases and dross generation during the preparation of master alloys are of great concern to the environment [8]. In order to overcome these difficulties, addition of oxide for refinement of grain is a commercially viable and environmental friendly method. Various novel refiners were produced till date and their significance on grain refinement was investigated extensively [9, 10]. However, research on a suitable replacement for commercial refiner is still to be carried out.

Oxides are thermodynamically stable and have good lattice match with the aluminium alloy and act an effective nucleant [11, 12]. Upon introduction of ultrasonic treatment (UT), these oxides tend to turn as heterogeneous nucleation spots that contribute for grain refinement [13]. Therefore, employment of oxide particles such as MgAl<sub>2</sub>O<sub>4</sub> [14], MgO [15] and Al<sub>2</sub>O<sub>3</sub> [14, 15] as nucleating agents is

✉ T. Satish Kumar  
satishmetly@gmail.com

<sup>1</sup> Department of Mechanical Engineering, Sri Ramakrishna Engineering College, Coimbatore, Tamilnadu, India

<sup>2</sup> Structural Nanomaterials Laboratory, PSG Institute of Advanced Studies, Coimbatore, Tamil Nadu 641 004, India

<sup>3</sup> Department of Metallurgical Engineering, PSG College of Technology, Coimbatore, Tamil Nadu 641 004, India

focused as they form oxides easily on surface of aluminium melt under different conditions. Amongst them,  $\text{MgAl}_2\text{O}_4$  is chosen for the study due to its effective refiner for nucleation owing to very small lattice mismatch (1.4%) and crystal structure similar to aluminium [11].

$\text{MgAl}_2\text{O}_4$  can be generated in situ through addition of oxide particles to the aluminium melt. Formation of in situ  $\text{MgAl}_2\text{O}_4$  in different metal matrix composites (MMCs) is extensively understood and any source of oxygen is suitable to generate  $\text{MgAl}_2\text{O}_4$  in Al–Mg alloy [16, 17]. Researchers have reported on addition of various oxides such as  $\text{Al}_2\text{O}_3$  [18],  $\text{SiO}_2$  [19],  $\text{TiO}_2$  [20],  $\text{MnO}_2$  [21] and generation of  $\text{MgAl}_2\text{O}_4$  particles resulting from the oxide reduction and Al and Mg consumption from matrix. Harini et al. [22] studied the efficiency of Al– $\text{MgAl}_2\text{O}_4$  master alloy synthesised from Al–2wt%Mg alloy and  $\text{SiO}_2$  (5 wt%) under UT. Results revealed two- to threefold grain size reduction with increase in  $\text{MgAl}_2\text{O}_4$  addition and 11–12-fold decrease in grain size upon UT. Horng [20] fabricated Al–4Mg/ $\text{Al}_2\text{O}_3$  composites through vortex method and remelted the composites at various temperatures of 700 °C, 750 °C, 800 °C and 850 °C for different times to investigate the generation of  $\text{MgAl}_2\text{O}_4$  spinel. Fine and uniform  $\text{MgAl}_2\text{O}_4$  particles were reported to be formed over the  $\text{Al}_2\text{O}_3$  particles.

Oxygen source like boric acid ( $\text{H}_3\text{BO}_3$ ) can be added to the aluminium melt by simple addition technique which can aid in complete reaction of the oxygen source. Also  $\text{H}_3\text{BO}_3$  is considered as a simpler and cheaper oxygen source. However, there are limited reports on  $\text{H}_3\text{BO}_3$  as precursor for generation of  $\text{MgAl}_2\text{O}_4$  composites. Hence, in this study, an attempt has been made to synthesize in situ Al– $\text{MgAl}_2\text{O}_4$  composite by addition of  $\text{H}_3\text{BO}_3$  in Al–4Mg alloy and there by  $\text{MgAl}_2\text{O}_4$  conversion into effective heterogeneous nucleating spots through UT. Therefore, in situ synthesis of  $\text{MgAl}_2\text{O}_4$  can help in significant grain refinement and enhancement in mechanical properties of Al–Mg alloy.

## 2 Materials and Methods

EC-grade pure aluminium (0.07 wt% Si, 0.1 wt% Fe, 0.005 wt% Ti and Al-bal) and commercial grade Mg (99.92 wt%) were used as starting materials.  $\text{H}_3\text{BO}_3$  powder with particle size of  $\sim 20 \mu\text{m}$  was used as the oxygen source for the in situ formation of  $\text{MgAl}_2\text{O}_4$ . Firstly, Al–4Mg alloy was prepared by dissolving 4 wt% of Mg in molten Al. Secondly,  $\text{H}_3\text{BO}_3$  powders were weighed to get different wt% (1, 2 and 3) of  $\text{MgAl}_2\text{O}_4$  and were preheated to remove moisture and any other volatile impurities. The preheated  $\text{H}_3\text{BO}_3$  powders were then added to the molten Al–4Mg alloy maintained at 750 °C. The

melt was maintained at 750 °C for 15 min and stirred at a regular interval of 5 min to enhance proper dissolution of  $\text{H}_3\text{BO}_3$  powders and to assist in situ reaction. Subsequently, the melt was treated with ultrasonic waves for 5 min. High-power ultrasonic wave generated using magnetostrictive transducer (RELTECH, Russia) with a frequency of 20.1 kHz and intensity ( $\sim 128 \text{ W/cm}^2$ ) were transmitted to the molten melt by using a SS304 Sonotrode (schematic illustration—Fig. 1). After ultrasonic treatment, the melt was cast into preheated cast iron moulds of diameter 20 mm and height 120 mm.

A separate set of alloy and composite melts without any ultrasonic treatment were prepared for comparison. To ensure generation of  $\text{MgAl}_2\text{O}_4$  and to study the morphology and distribution of  $\text{MgAl}_2\text{O}_4$ , specimens from the composite were cut, ground, polished, and electrochemically etched using  $\text{HBF}_4$  solution (with 20 V DC for 60 s) and analysed with Carl Zeiss EVO 18 SEM. The effect of  $\text{MgAl}_2\text{O}_4$  and UT on grain refinement was analysed using a polarized light microscope. A standard tensile sample of 20 mm gauge length was prepared from the alloy and composites and tensile analysis was carried out by Instron 3366 UTM with an initial strain rate of  $4.16 \times 10^{-4} \text{ s}^{-1}$ . An average of four set of data are shown as the tensile results.

## 3 Results

### 3.1 Role of UT on Generation of In Situ Reinforcement Particles

The in situ  $\text{MgAl}_2\text{O}_4$  are generated by boric acid ( $\text{H}_3\text{BO}_3$ ) reduction through the following displacement reactions.

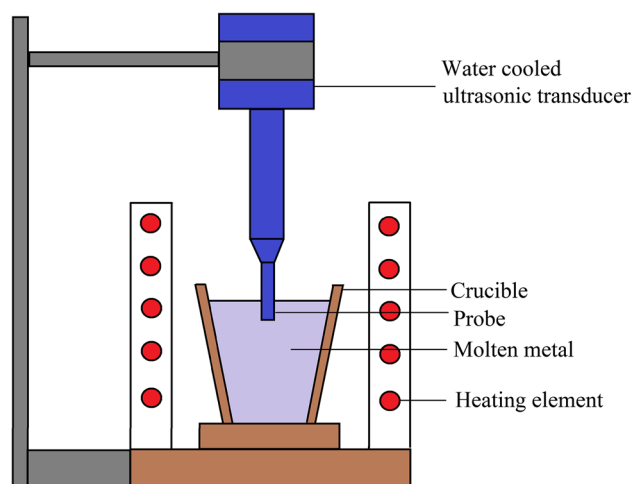
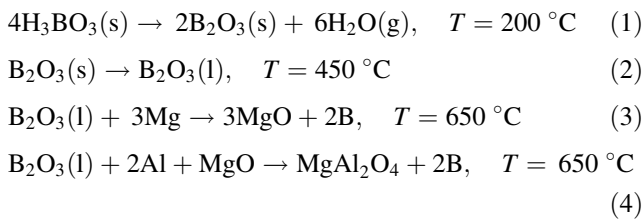


Fig. 1 Illustration of ultrasonic setup



Segregation of solute occurs usually on the melt surface. In Al–Mg alloys, elemental Mg gets favourably segregated and oxidizes at high temperature which is required for the formation of in situ reinforcement particles. Any specific processing temperature that is required for the continuation of reduction reaction results from series of reactions mentioned in Eqs. (1)–(4).

Microstructure of Al–4Mg/3 wt% MgAl<sub>2</sub>O<sub>4</sub> composites is shown in Fig. 2. The SEM microstructure of the composites with and without UT indicates the occurrence of polygonal faceted-type MgAl<sub>2</sub>O<sub>4</sub> in α-aluminium matrix. Formation of both MgO and MgAl<sub>2</sub>O<sub>4</sub> crystals is perceived in the composite specimens without any ultrasonic treatment (Fig. 2a). The UT composite reveals only the occurrence of MgAl<sub>2</sub>O<sub>4</sub> spinel crystals whereas the presence of MgO particles is not observed in the same. The size of MgAl<sub>2</sub>O<sub>4</sub> particles in Al–4Mg/3MgAl<sub>2</sub>O<sub>4</sub> composite without UT are estimated as 2.5 ± 0.65 μm while the size

of MgAl<sub>2</sub>O<sub>4</sub> particle in composite with UT has been found to be reduced to 315 ± 62 nm. The MgAl<sub>2</sub>O<sub>4</sub> in composite specimens with UT are observed as well dispersed amongst the matrix along with the particle refinement.

### 3.2 Role of UT on Grain Refinement of Al–4Mg/MgAl<sub>2</sub>O<sub>4</sub> Composites and Nucleation Efficiency of MgAl<sub>2</sub>O<sub>4</sub>

Figure 3 shows the microstructure of Al–4Mg base matrix alloy and its composites. The microstructure reveals the formation of dendritic pattern on solidification. A substantial decrease in grain size of composites is noted in contrast to base alloy. UT is further found to extend the refinement of grain size in composite samples. Absence of columnar structure in composite specimen ensures the occurrences of heterogeneous nucleation in the sample.

It is evident from the microstructures that the presence of MgAl<sub>2</sub>O<sub>4</sub> and ultrasonic treatment has substantial effect on grain refinement of the alloy. Presence of MgAl<sub>2</sub>O<sub>4</sub> has been proved to induce a refinement in grain size of the alloy and the grain size is found to reduce from 1237 to ~ 660 μm. In case of UT, the grain size further reduces to ~ 460 μm. The presence of 3 wt% MgAl<sub>2</sub>O<sub>4</sub> particles and ultrasonic cavitation effect reduces the grain size of alloy up to ~ 250 μm.

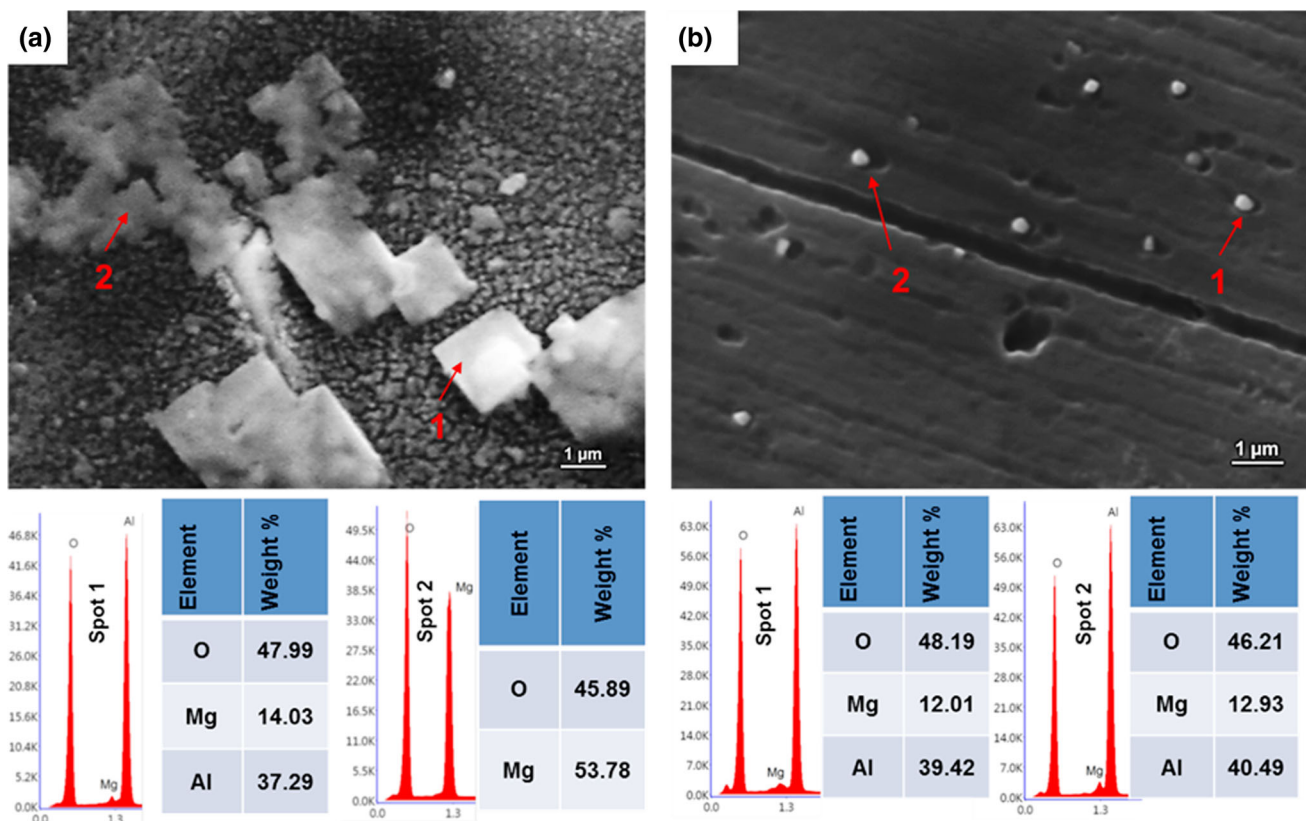
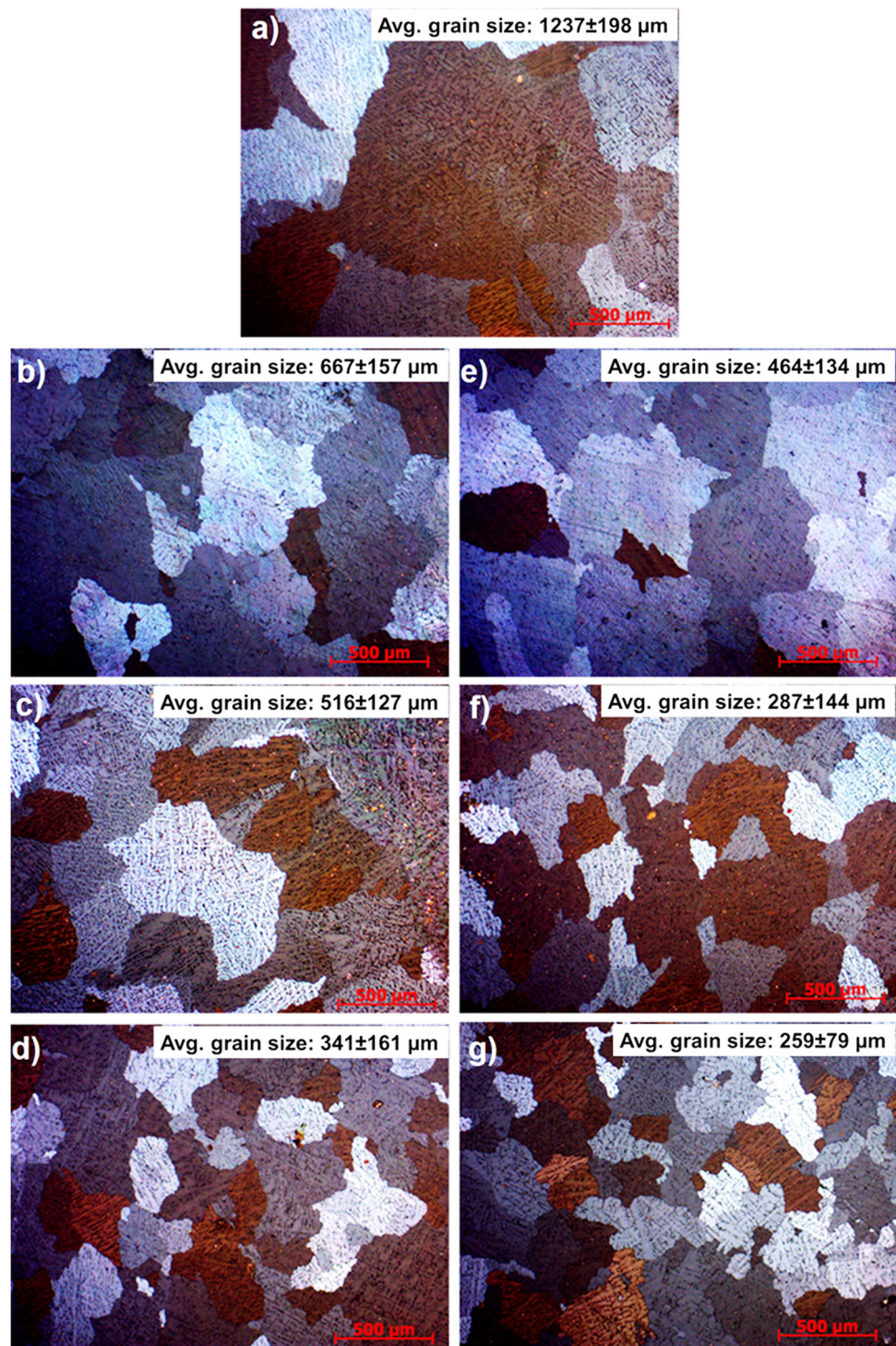


Fig. 2 SEM microstructure of Al–4Mg/3wt% MgAl<sub>2</sub>O<sub>4</sub> a without UT and b with UT

**Fig. 3** Optical microstructure of **a** Al–4Mg alloy, Al–4Mg/x wt% MgAl<sub>2</sub>O<sub>4</sub> composite without UT, **b** 1 wt%, **c** 2 wt%, **d** 3 wt% and Al–4Mg/x wt% MgAl<sub>2</sub>O<sub>4</sub> composite with UT **e** 1 wt%, **f** 2 wt%, **g** 3 wt%



### 3.3 Role of MgAl<sub>2</sub>O<sub>4</sub> and UT on the Morphology and Size of $\beta$ -Phase

Along with the refinement of Al–4Mg alloy, refinement in secondary phase ( $\beta$  phase) is also attained in composite specimens with and without UT (Fig. 4). The  $\beta$  phase particles in the alloy appear with an acicular morphology

with size and aspect ratio of  $22 \pm 5.7 \mu\text{m}$  and  $8.8 \pm 0.7$ , respectively. The occurrence of MgAl<sub>2</sub>O<sub>4</sub> refines the  $\beta$  phase into small particles of size  $4.47 \pm 0.67 \mu\text{m}$  and aspect ratio of  $5.02 \pm 0.98$ . UT of composite further refines the secondary phases to  $2.2 \pm 0.45 \mu\text{m}$  with an aspect ratio of  $2.7 \pm 1$ . Microstructure shows the occurrence of MgAl<sub>2</sub>O<sub>4</sub>, and ultrasonic treatment is found to

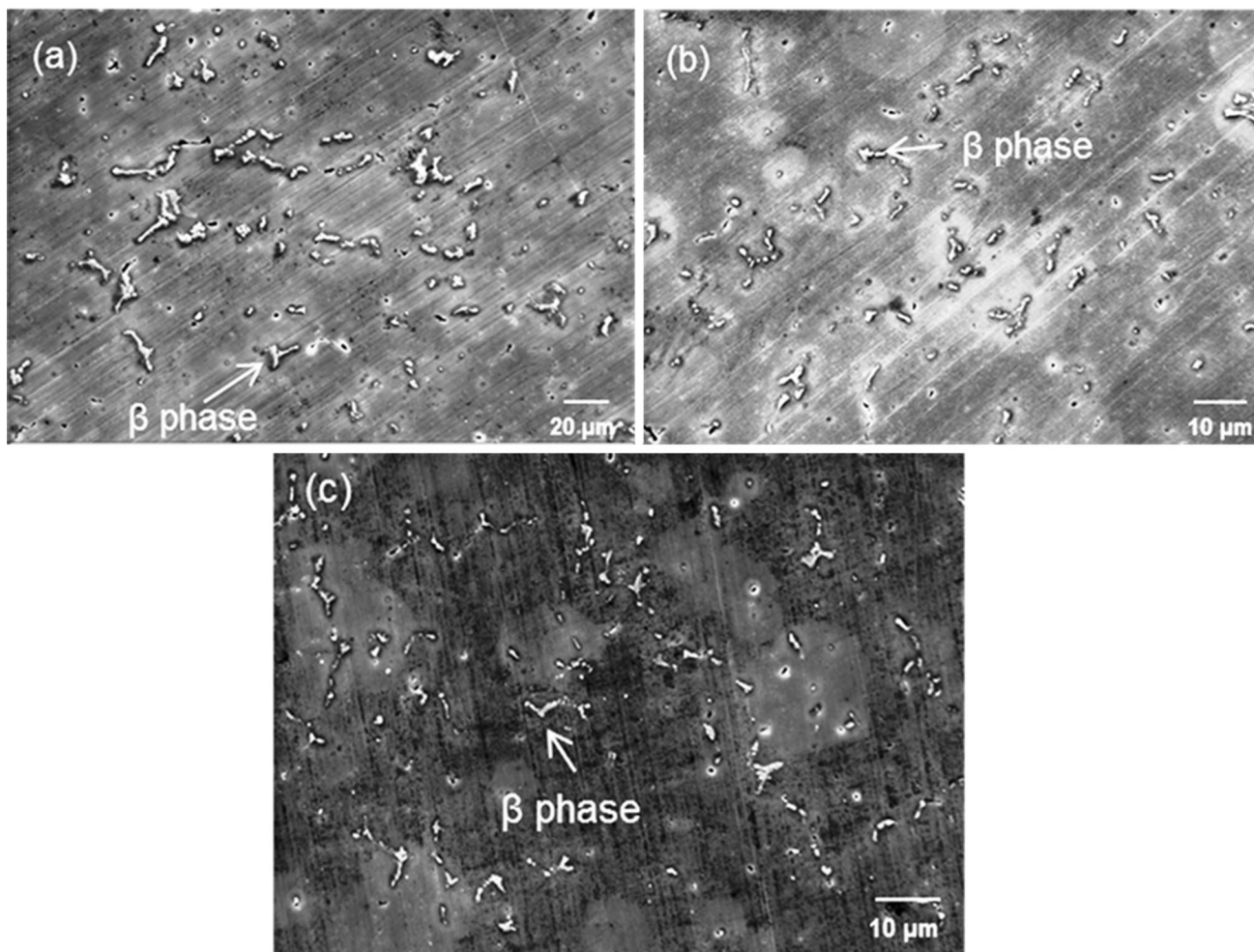


**Fig. 4** SEM micrograph of **a** Al–4Mg alloy, **b** Al–4Mg/3MgAl<sub>2</sub>O<sub>4</sub> composite without UT and **c** Al–4Mg/3MgAl<sub>2</sub>O<sub>4</sub> composite with UT phase

have substantial effect on generation of secondary phases. The mechanism of generation of secondary phases will be explained in the forthcoming sections.

### 3.4 Mechanical Properties of Al–4Mg/MgAl<sub>2</sub>O<sub>4</sub> Composites

#### 3.4.1 MicroVickers Hardness of Al–4Mg/MgAl<sub>2</sub>O<sub>4</sub> Composites

The microhardness of the composite (with and without UT) is depicted in Fig. 5. It is observed that increase in wt% of MgAl<sub>2</sub>O<sub>4</sub> increases the hardness of composite in both conditions of the alloy (with and without UT). The hardness is found to increase from a minimum value of 66 HV for (alloy) to a maximum value of 80 HV in the Al–4Mg/MgAl<sub>2</sub>O<sub>4</sub> composite with UT which is due to more generation of MgAl<sub>2</sub>O<sub>4</sub> upon H<sub>3</sub>BO<sub>3</sub> addition. MgAl<sub>2</sub>O<sub>4</sub> particles generally possess high hardness due to its hard ceramic phase and further, the in situ MgAl<sub>2</sub>O<sub>4</sub> is

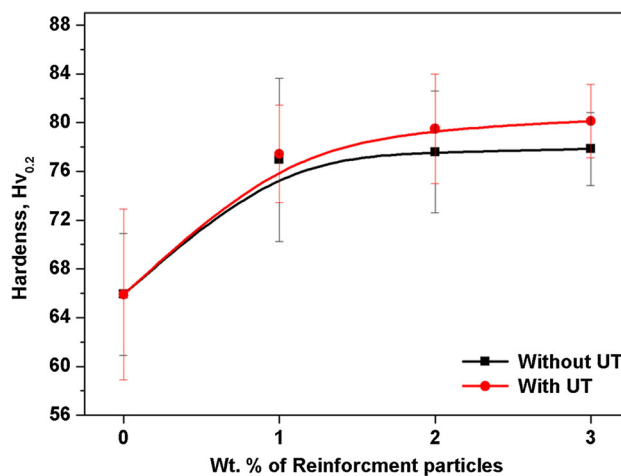


**Fig. 5** Hardness survey of Al–4Mg/MgAl<sub>2</sub>O<sub>4</sub> composites with and without ultrasonic treatment

extremely effective in transferring the load from matrix to reinforcement, there by resulting in higher hardness.

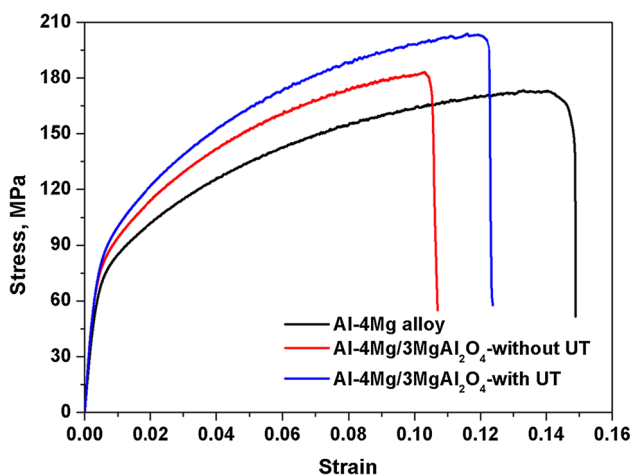


**Fig. 6** Stress–strain behaviour of Al–4Mg alloy and Al–4Mg/MgAl<sub>2</sub>O<sub>4</sub> composites with and without UT

### 3.4.2 Room-Temperature Tensile Performance of Al–4Mg/MgAl<sub>2</sub>O<sub>4</sub> Composites

Figure 6 shows the room-temperature stress–strain curve of Al–4Mg monolithic alloy and Al–4Mg/MgAl<sub>2</sub>O<sub>4</sub> composites. Monolithic Al–4Mg alloy possess an average yield strength and ultimate tensile strength (UTS) of  $\sim 72$  MPa and  $\sim 178$  MPa, respectively. A considerable improvement in yield strength, UTS and toughness (area under the curve) for the composites is noticed from the stress–strain curve. The composite specimen without UT exhibits average yield strength and UTS of  $\sim 80$  MPa and 183 MPa, respectively, with a reduction in ductility. The toughness (area under the curve) of the composite samples prepared without UT is also lesser than that of monolithic alloy. The reduction in elongation at break and toughness is ascribed to the presence of and allied stress riser effect of partially converted MgO agglomerates and micron sized MgAl<sub>2</sub>O<sub>4</sub> particles. UT of composite samples enhances the yield strength and UTS to  $\sim 87$  MPa and  $\sim 204$  MPa, respectively, with substantial retention in ductility and toughness. The retention in of ductility and toughness (area under curve) of the composite specimen with UT is ascribed to increase in conversion of MgO into MgAl<sub>2</sub>O<sub>4</sub> particles, refinement in MgAl<sub>2</sub>O<sub>4</sub> size and breakage and distribution of agglomerated particles by UT. The results of tensile analysis are summarized in Table 1 for quick reference.

## 4 Discussions

### 4.1 Formation of MgAl<sub>2</sub>O<sub>4</sub> Particles with and Without UT

Generation of in situ MgAl<sub>2</sub>O<sub>4</sub> in Al–4Mg–H<sub>3</sub>BO<sub>3</sub> is discussed according to displacement reactions and cavitation

**Table 1** Effect of UT on tensile properties of Al–4Mg alloy and its composites

Sample name	Yield strength (MPa)	Ultimate tensile strength (MPa)
Al–4Mg	72	178
Al–4Mg/MgAl <sub>2</sub> O <sub>4</sub> without UT	80	183
Al–4Mg/MgAl <sub>2</sub> O <sub>4</sub> with UT	87	204

implosion phenomena of ultrasonic waves. In Al–4Mg/3MgAl<sub>2</sub>O<sub>4</sub> composite without UT, formation of both MgO and MgAl<sub>2</sub>O<sub>4</sub> crystals is observed with agglomeration of MgO crystals. According to displacement reactions, when the primary layer of MgAl<sub>2</sub>O<sub>4</sub> forms over MgO, the atoms of Al from matrix and O from B<sub>2</sub>O<sub>3</sub> should diffuse at the interface in order for the reaction to proceed. The formed MgAl<sub>2</sub>O<sub>4</sub> can act as a barrier to hinder the further diffusion of Al and O which may retard the displacement reactions. This occurrence can be attributed to the partial conversion of MgO–MgAl<sub>2</sub>O<sub>4</sub>. When ultrasonic waves are passed into the melt, they produce acoustic cavitation and streaming effects. Formation, development and breakdown of cavitation bubbles result in acoustic cavitation upon alternate acoustic pressure wave cycles [23]. Several tiny cavities are generated by the gases on oxide surface and get imploded beyond a threshold which results in the development of higher pressure and temperature at the locality of the implosion. Hence the surface reaction is improved on the melt upon the gas implosion due to cavitation bubble's growth. Liquid jets are produced simultaneously and impinges at higher speed on the surface for the removal of reaction products. Micro-jets with the velocity range of 200–700 m/s are generated upon implosion of cavitation bubbles [24]. Micro-jets of liquid can remove the layer of MgAl<sub>2</sub>O<sub>4</sub> from the surface of MgO surface, and the fresh surface of MgO gets exposed in order to complete the displacement reaction. Research reveals that higher pressure resulting due to acoustic cavitation in molten aluminium can promote the cluster de-agglomeration [25]. The agglomerates of MgAl<sub>2</sub>O<sub>4</sub> crystals are bonded by van der Waals force mainly to reduce the surface energy, and it could be de-agglomerated by the inducing external fields like the pressure shock waves and micro-jet streaming of cavitation implosion. Thus, the agglomerated particles are separated and turned into finer particles of size  $2.5 \pm 0.65 \mu\text{m}$  (without UT) to  $315 \pm 62 \text{ nm}$  (with UT). In a nutshell, cavitation implosion and acoustic streaming effect of UT enhances the rate of reaction that can complete the conversion of H<sub>3</sub>BO<sub>3</sub> into MgAl<sub>2</sub>O<sub>4</sub> and improves the particle distribution.

## 4.2 Role of MgAl<sub>2</sub>O<sub>4</sub> and UT on Grain Refinement of Al–4Mg/MgAl<sub>2</sub>O<sub>4</sub> Composites

Substantial decrease in grain size is observed in Al–4Mg/MgAl<sub>2</sub>O<sub>4</sub> composites with and without UT. This is ascribed to the enhanced heterogeneous nucleation of  $\alpha$ -Al on the MgAl<sub>2</sub>O<sub>4</sub> particle's surface and localized undercooling effect provided by UT in the melt. Studies show that MgAl<sub>2</sub>O<sub>4</sub> can operate as effective substrate for heterogeneous nucleation of aluminium grains owing to its cube-on-cube orientation relationship [13, 16]. As per classical nucleation theory, this potent nucleant decreases the barrier for activation of nucleation. This activation barrier is decided by interfacial energy of the nucleant/nucleus metal for heterogeneous nucleation. The decrease in activation barrier level is influenced by the contact angle between the nucleant and the nucleating phase. The contact angle is an important parameter, and it should be low for effective nucleation [26].

Low lattice mismatch between the nucleant and the nucleating phase decreases the interfacial energy and helps in achieving low contact angle. Hence, MgAl<sub>2</sub>O<sub>4</sub> particles become a potential nucleant owing to the small lattice mismatch and face-centred cubic structure which is similar to that of aluminium [27]. Similar crystal structures form low-energy interfaces for any orientation. For (111) plane along [110] direction, extremely small mismatch of 1.41% between aluminium and MgAl<sub>2</sub>O<sub>4</sub> is observed [13]. However, low lattice mismatch makes MgAl<sub>2</sub>O<sub>4</sub> a potent nucleant, and the potency also depends on numerous parameters such as adequate number density, particle size and narrow size distribution for heterogeneous nucleation. Enormous undercooling is essential for smaller particles which greatly influences the growth of grains [28]. Athermal heterogeneous nucleation theory is given in Eq. (5) [29]

$$\Delta T = 4\Gamma_{sl}/D \quad (5)$$

where  $\Delta T$  is nucleation undercooling,  $\Gamma_{sl}$  is Gibbs–Thomson coefficient between the liquid and the solid embryo of the solid phase,  $D$  is the particle diameter.

In contrary, UT aids in overcoming aforementioned difficulties by enhancing the number density and undercooling for smaller particles. MgAl<sub>2</sub>O<sub>4</sub> size is reduced to 1  $\mu\text{m}$  in composite specimen with UT. Undercooling for 1  $\mu\text{m}$  MgAl<sub>2</sub>O<sub>4</sub> crystals according to (Gibbs–Thomson coefficient, with  $\Gamma_{sl}$  of aluminium alloy as  $9.12 \times 10^{-8}$  K m, is calculated as 0.3 K. The microstructures substantiate that the essential undercooling for nucleation of grains is provided by UT and helps in refinement of the alloy. The grain refinement by UT is explained through two mechanisms (1) cavitation-enhanced nucleation and (2) cavitation-induced dendrite

fragmentation. Cavitation-enhanced heterogeneous nucleation is the anticipated mechanism for refinement in agreement with the development of uniform equiaxed grains upon UT. Further, pressure pulse–melting point [30] and cavitation-induced wetting cavitation are the two different mechanisms which are the cause for enhanced heterogeneous nucleation. According to Clapeyron equation [31], cavitation implosion generates a pressure pulse that modifies the melting point of alloy ( $T_m$ ), in pressure pulse–melting point mechanism. Increase in  $T_m$  provides localized undercooling and therefore it improves the nucleation potency of particles [32, 33]. In case of cavitation-induced wetting cavitation, pressure pulse causes the melt to fill the cracks and cavities on the substrate surfaces and turns these defects into active nucleation sites.

The refinement of secondary  $\beta$ -phase is due to growth hindrance effect of MgAl<sub>2</sub>O<sub>4</sub> particles. This particle turns as pinning agent for the development of secondary phases. Upon UT, the number density of particles is increased to pin on grain boundaries to further prevent the enlargement of  $\beta$ -phase size.

## 4.3 Strengthening Mechanisms

Mechanical properties are influenced by MgAl<sub>2</sub>O<sub>4</sub> formation and are likely attributed to the strengthening mechanism—which is dominant in composites. Such mechanism is grain boundary strengthening, load-bearing strengthening, coefficient of thermal expansion (CTE) mismatch strengthening and Orowan dispersion strengthening [15, 34].

The strength increment in composite and retention of elongation with UT is due to the refinement of  $\beta$  phase. The  $\beta$  phase shows large acicular needle shape in the unreinforced Al–Mg alloy, whereas in the Al–4Mg/MgAl<sub>2</sub>O<sub>4</sub> composite sample without UT, there is a slight refinement of secondary  $\beta$  phase. In case of composites with UT, greater refinement of  $\beta$  phase takes place and morphology gets changed as fine faceted which contributes to the improved ductility.

As per Hall–Petch theory, strength improvement is due to grain boundary strengthening mechanism [34]. The Al–4Mg/MgAl<sub>2</sub>O<sub>4</sub> composites (with and without UT) have refined grain size and eventually more grain boundaries as compared to unreinforced alloy. The dislocations move through lattice during deformation, and its movement is inhibited by the grain boundaries. The movement of dislocation is restricted further because the grain boundaries tend to operate as the pinning points. As more number of dislocation moves towards the grain boundary, pile up of dislocation takes place. Hence further deformation is resulted under pile up action which force the dislocations to shift across the grain boundary. The extent of pile up is

reduced by smaller grain size and large number of grain boundaries in the Al–4Mg/MgAl<sub>2</sub>O<sub>4</sub> composites due to different orientation of nearby grains in the matrix which makes movement of dislocation difficult. Thus it can be concluded that grain refinement greatly contributes to strengthening of the composites.

Orowan dispersion strengthening is predominant in composites, and it greatly depends on the bonding between the reinforcement and the matrix, particles size and inter-particle distance [34]. During deformation, softer primary phase (Al) deforms plastically as compared to harder secondary phase MgAl<sub>2</sub>O<sub>4</sub> particles. The dislocation movement during deformation of primary phase is hindered by nearly spaced MgAl<sub>2</sub>O<sub>4</sub> reinforcement particles and dislocations are unable to pass the MgAl<sub>2</sub>O<sub>4</sub> since it is stronger than Al matrix. Thus dislocation bending takes place which produces loop around MgAl<sub>2</sub>O<sub>4</sub> particles and makes dislocation movement hard. Successive dislocation continuously forms loop around MgAl<sub>2</sub>O<sub>4</sub> particles which induces back stress and impedes dislocation movement further. This act of MgAl<sub>2</sub>O<sub>4</sub> particles helps in strengthening of matrix. The inter-particle distance is inversely proportional to the resistance to dislocation motion. The relatively smaller inter-particle distance in the Al–4Mg/MgAl<sub>2</sub>O<sub>4</sub> composite (with UT) strengthens the matrix highly compared to the Al–4Mg/MgAl<sub>2</sub>O<sub>4</sub> composite (without UT).

The load-bearing strengthening mechanism has a direct influence on the reinforcement particles. This strengthening occurs on load transfer from matrix to reinforcement particles. The greater bonding between matrix and reinforcement can efficiently take part in effective load transfer [17]. Higher strength attained in the Al–4Mg/2H<sub>3</sub>BO<sub>3</sub> composite (with UT) implies that greater bonding exists between MgAl<sub>2</sub>O<sub>4</sub> particles and the aluminium matrix.

CTE mismatch strengthening occurs owing to greater difference in thermal expansion coefficient between the matrix and the reinforcement [17]. Since  $\alpha$  of Al alloy ( $25 \times 10^{-6}/\text{K}$ ) and  $\alpha$  of MgAl<sub>2</sub>O<sub>4</sub> ( $8.1 \times 10^{-6}/\text{K}$ ) has larger difference, stresses may built up on cooling and consequence in dislocations near to MgAl<sub>2</sub>O<sub>4</sub>—reinforcement particles. This action enhances the strength of matrix and it also relies on volume fraction and particle size of reinforcement.

## 5 Conclusion

In situ MgAl<sub>2</sub>O<sub>4</sub> were successfully synthesized in Al–4Mg alloy through addition of H<sub>3</sub>BO<sub>3</sub> precursor assisted by ultrasonic treatment. The extent of MgAl<sub>2</sub>O<sub>4</sub> generation and distribution was enhanced by ultrasonic treatment. MgAl<sub>2</sub>O<sub>4</sub> particles acted as latent nucleating spots owing to

its lattice matching with Al. A decrease of 3–4 times in grain size was perceived in Al–4Mg alloy, and grain refinement of 5–6 times was attained in Al–4Mg alloy under ultrasonic treatment. Constitutional undercooling established pressure–pulse melting was proposed as a mechanism behind the refinement of grains with UT. Hardness and tensile strength of the Al–4Mg/MgAl<sub>2</sub>O<sub>4</sub> composites was observed to be higher than unreinforced alloy and improved with increase in wt% of H<sub>3</sub>BO<sub>3</sub>. Grain boundary strengthening, Orowan dispersion strengthening, load bearing and coefficient of thermal expansion mismatch strengthening were the anticipated mechanisms for enhanced mechanical properties of the Al–4Mg/MgAl<sub>2</sub>O<sub>4</sub> composites.

**Acknowledgements** One of the authors (JN) would like to thank the Council of Scientific and Industrial Research, New Delhi, for the Senior Research Fellowship (Award No.: 08/473(0006)/2015 EMR-1).

**Data Availability** The raw/processed data required to reproduce these findings cannot be shared at this time as the data also forms part of an ongoing study.

## References

1. McCartney D G, *Int Mater Rev* **34** (1989) 247.
2. Mayes C D, McCartney D G, and Tatlock G J, *Mater Sci Eng* **188** (1994) 283.
3. Wannasin J, Canyook R, Wisutmethangoon S, and Flemings M C, *Acta Mater* **61** (2013) 3897.
4. Easton M, St John D, *Metall Mater Trans A* **30A** (1999) 1613.
5. Mohanty P S, and Gruzleski J E, *Acta Mater* **44** (1996) 3749.
6. Mohanty P S, and Gruzleski J E, *Acta Mater* **43** (1995) 2001.
7. Prasad A, Mok J, Lafortune L, Bichler L, *Trans Indian Inst Met* **71** (2018) 2759.
8. Kotadia H R, Qian M, and Das S, *Trans Indian Inst Met* **71** (2018) 2681.
9. Lindsay G, Coope P S, Meredith MW, Schneider W, Schumacher P, Spittle J A, and Tronche A, *Adv Eng Mater* **5** (2003) 81.
10. Yucel Birol, *J Alloys Compd* **443** (2007) 94.
11. Kori S A, Murty B S, and Chakraborty M, *Mater Sci Eng A* **283** (2000) 94.
12. Prasada Rao A K, Das K, Murty B S, and Chakraborty M, *J Alloys Compd* **480** (2009) 49.
13. Li H T, Wang Y, and Fan Z, *Acta Mater* **60** (2012) 1528.
14. Sun J, Wang D, Zhang Y, Sheng C, Dargusch M, Wang G, St John D, and Zhai Q, *J Alloys Compd* **753** (2018) 543.
15. Zuo Y, Li H, Xia M, Jiang B, Scamans G M, and Fan Z, *Scr Mater* **64** (2011) 209.
16. Wang Y, Li H-T, Fan Z, *Trans Indian Inst Met* **65** (2012) 653.
17. Sreekumar V M, Babu N H, and Eskin D G, *J Mater Eng Perform* **26** (2017) 4166.
18. Kim K H, *Mater Lett* **117** (2014) 74.
19. Sreekumar V M, Hari Babu N, Eskin D G, and Fan Z, *Mater Sci Eng A* **628** (2015) 30.
20. Hornig C-F, Lin S-J, and Liu K-S, *Mater Sci Eng A* **150** (1992) 289.
21. Tsunekawa Y, Suzuki H, and Genma Y, *Mater Des* **22** (2001) 467.



22. Harini R S, Raj B, and Ravi K R, *Trans Indian Inst Met* **68** (2015) 1059.
23. Leighton T G, *J Fluid Mech* **272** (1994) 407.
24. Tzanakis I, Lebon G S B, Eskin D G, and Pericleous K, *J Mater Process Technol* **229** (2016) 582.
25. Tzanakis I, Eskin D G, Georgoulas A, and Fytanidis D K, *Ultrason Sonochem* **21** (2014) 866.
26. Harini R S, Nampoothiri J, Nagasivamuni B, Raj B, and Ravi K R, *Mater Lett* **145** (2015) 328.
27. Kim KH, *Surf Interface Anal* **47** (2015) 429.
28. Greer A L, Bunn A M, Tronche A, Evans P V, and Bristow D J, *Acta Mater* **48** (2000) 2823.
29. Sreekumar V M, Babu N H, and Eskin D G, *Metall Mater Trans B* **48** (2016) 208.
30. Hunt J D, and Jackson K A, *J Appl Phys* **37** (1966) 254.
31. Raghu R, Nampoothiri J, and Satish Kumar T, *Measurement* **129** (2018) 389.
32. Nampoothiri J, Raj B, and Ravi K R, *Trans Indian Inst Met* **68** (2015) 1101.
33. Ramirez A, Qian M, Davis B, Wilks T, St John D H, *Scr Mater* **59**, 19 (2008).
34. Karbalaee Akbari M, Baharvandi H R, and Shirvanimoghaddam K, *Mater Des* **66** (2015) 150.

#### Publisher's Note

Springer Nature remains neutral with regard to jurisdictional claims in published maps and institutional affiliations.